NASA/TP—2008-214818

# Electromagnetic Forces in a Hybrid Magnetic-Bearing Switched-Reluctance Motor

*Carlos R. Morrison*
*Glenn Research Center, Cleveland, Ohio*

*Mark W. Siebert*
*University of Toledo, Toledo, Ohio*

*Eric J. Ho*
*University of Texas at Arlington, Arlington, Texas*

March 2008

# NASA STI Program . . . in Profile

Since its founding, NASA has been dedicated to the advancement of aeronautics and space science. The NASA Scientific and Technical Information (STI) program plays a key part in helping NASA maintain this important role.

The NASA STI Program operates under the auspices of the Agency Chief Information Officer. It collects, organizes, provides for archiving, and disseminates NASA's STI. The NASA STI program provides access to the NASA Aeronautics and Space Database and its public interface, the NASA Technical Reports Server, thus providing one of the largest collections of aeronautical and space science STI in the world. Results are published in both non-NASA channels and by NASA in the NASA STI Report Series, which includes the following report types:

- TECHNICAL PUBLICATION. Reports of completed research or a major significant phase of research that present the results of NASA programs and include extensive data or theoretical analysis. Includes compilations of significant scientific and technical data and information deemed to be of continuing reference value. NASA counterpart of peer-reviewed formal professional papers but has less stringent limitations on manuscript length and extent of graphic presentations.

- TECHNICAL MEMORANDUM. Scientific and technical findings that are preliminary or of specialized interest, e.g., quick release reports, working papers, and bibliographies that contain minimal annotation. Does not contain extensive analysis.

- CONTRACTOR REPORT. Scientific and technical findings by NASA-sponsored contractors and grantees.

- CONFERENCE PUBLICATION. Collected papers from scientific and technical conferences, symposia, seminars, or other meetings sponsored or cosponsored by NASA.

- SPECIAL PUBLICATION. Scientific, technical, or historical information from NASA programs, projects, and missions, often concerned with subjects having substantial public interest.

- TECHNICAL TRANSLATION. English-language translations of foreign scientific and technical material pertinent to NASA's mission.

Specialized services also include creating custom thesauri, building customized databases, organizing and publishing research results.

For more information about the NASA STI program, see the following:

- Access the NASA STI program home page at *http://www.sti.nasa.gov*

- E-mail your question via the Internet to *help@sti.nasa.gov*

- Fax your question to the NASA STI Help Desk at 301–621–0134

- Telephone the NASA STI Help Desk at 301–621–0390

- Write to:
  NASA Center for AeroSpace Information (CASI)
  7115 Standard Drive
  Hanover, MD 21076–1320

NASA/TP—2008-214818

# Electromagnetic Forces in a Hybrid Magnetic-Bearing Switched-Reluctance Motor

*Carlos R. Morrison*
*Glenn Research Center, Cleveland, Ohio*

*Mark W. Siebert*
*University of Toledo, Toledo, Ohio*

*Eric J. Ho*
*University of Texas at Arlington, Arlington, Texas*

National Aeronautics and
Space Administration

Glenn Research Center
Cleveland, Ohio 44135

March 2008

## Acknowledgments

The motor was developed with support from the NASA Strategic Research Fund (SRF) Combined Motor/Magnetic Bearing Project (Dr. Marvin Goldstein, manager); from the Revolutionary Aeropropulsion Concept (RAC) Project, High Power Density Motors for Aircraft Propulsion (Mr. Leo Burkardt, manager); and subsequently from the Alternate Fuel Foundation Technology (AFFT) with Mr. Dave Ercegovic as project manager. Special recognition is extended to Dr. Gerald V. Brown for his many insightful discussions that ultimately led to the theoretical analysis presented in this paper, Mr. Ben Ebihara and Mr. Carl Buccieri for their contributions in fabricating the motor, and Mr. Joseph Wisniewski and Mr. Gerald Buchar for their assistance with the motor's electrical and electronics wiring.

This work was sponsored by the Fundamental Aeronautics Program at the NASA Glenn Research Center.

*Level of Review*: This material has been technically reviewed by expert reviewers.

Available from

NASA Center for Aerospace Information
7115 Standard Drive
Hanover, MD 21076–1320

National Technical Information Service
5285 Port Royal Road
Springfield, VA 22161

Available electronically at http://gltrs.grc.nasa.gov

# Electromagnetic Forces in a Hybrid Magnetic-Bearing Switched-Reluctance Motor

Carlos R. Morrison
National Aeronautics and Space Administration
Glenn Research Center
Cleveland, Ohio 44135

Mark W. Siebert[1]
University of Toledo
Toledo, Ohio 43606

Eric J. Ho
University of Texas at Arlington
Arlington, Texas 76019

## Summary

Analysis and experimental measurement of the electromagnetic force loads on the hybrid rotor in a novel hybrid magnetic-bearing switched-reluctance motor (MBSRM) have been performed. A MBSRM has the combined characteristics of a switched-reluctance motor and a magnetic bearing. The MBSRM discussed in this report has an eight-pole stator and a six-pole hybrid rotor, which is composed of circular and scalloped lamination segments. The hybrid rotor is levitated using only one set of four stator poles, while a second set of four stator poles imparts torque to the scalloped portion of the rotor, which is driven in a traditional switched reluctance manner by a processor. Static torque and radial force analysis were done for rotor poles that were oriented to achieve maximum and minimum radial force loads on the rotor. The objective is to assess whether simple one-dimensional magnetic circuit analysis is sufficient for preliminary evaluation of this machine, which may exhibit strong three-dimensional electromagnetic field behavior. Two magnetic circuit geometries, approximating the complex topology of the magnetic fields in and around the hybrid rotor, were employed in formulating the electromagnetic radial force equations. Reasonable agreement between the experimental and the theoretical radial force loads predictions was obtained with typical magnetic bearing derating factors applied to the predictions.

## Introduction

There is a need for reliable, fail-safe, robust, compact, low-cost electric motors for applications with high temperatures or extreme temperature variations; switched-reluctance motors possess these characteristics (ref. 1). These motors have been evaluated as high-speed starter-generators (refs. 2 and 3). However, conventional switched-reluctance motors can suffer from undesired vibration due to (1) unbalanced lateral forces on the rotor caused by electrical faults, (2) mechanical offset of the rotor, and (3) uncontrolled pulsed current in one or more shorted coils (ref. 4). A viable solution for mitigating mechanical vibration is to suspend the rotor magnetically via magnetic levitation. In addition, magnetic suspension of the rotor allows the motor to operate at a much higher rotational frequency for a prolonged period. This benefit is due largely to the elimination of friction, as there is no physical contact between the stator and rotor. Consequently, motors incorporating magnetic bearings perform at higher efficiency than motors incorporating ball bearings. Magnetic levitation also obviates the need for a lubrication system, which has the added benefit of significantly decreasing the weight and complexity of turbomachinery mechanisms.

Methods for simultaneously levitating and rotating a rotor within a single stator in switched-reluctance motors have been proposed in references 5 and 6. In these motors, the technique of using differential stator windings was employed. The studies in references 5 and 6 center primarily around the use of a main four-pole winding to rotate an eight-pole rotor while utilizing a two-pole winding to apply radial force to the rotor with all of the 12 stator poles having both windings thereon. A variation on this theme was described in reference 7, wherein only a single coil on each stator pole (in a 12/8 stator-rotor pole configuration) was employed to achieve motor-bearing action.

Self-levitation (also called self-bearing) of motors has been achieved for nearly every type of electric motor, but is very marginal in performance for switched-reluctance motors with low numbers of poles. The motoring technique disclosed in

[1]Mark W. Siebert is currently with Cleveland State University, Cleveland, Ohio.

reference 8 will simultaneously levitate and rotate a rotor, not only for (18/12) and (12/8) stator-rotor pole combinations, but also for (8/6) and (6/4) configurations while employing a single set of coils positioned on each stator pole. The motoring techniques described in references 5 to 7 are not applicable to motors having low stator-rotor pole configuration of (8/6) or (6/4) because of the dearth of stator-rotor poles in appropriate positions to apply levitating forces. The hybrid rotor technique described in reference 8 will assure robust bearingless operation in all four aforementioned stator-rotor pole configurations. With circular laminations on the shaft, levitating force is always assured as the rotor spins.

A disassembled eight-pole stator, six-pole hybrid rotor (motor) is shown in figure 1. The rotor lamination stack has a cylindrical portion of its length (indicated by the left arrow in the picture) used for levitation and a scalloped portion (indicated by the right arrow) used for both levitation and motoring. An algorithm that handles both the levitating and motoring functions (ref. 8) controls the currents in the coils on the eight-pole stator. During normal operation, two pairs of opposing stator poles (at right angles to each other) levitate the rotor. The remaining two pairs of stator poles exert torque on the six-pole rotor lamination stack to produce rotation. The relative lengths of the circular and multipole lamination stacks on the rotor can be chosen to tailor the performance of the motor for a specific application. For a given overall length, increasing the length of the multipole stack relative to the circular stack results in an increase in torque relative to levitation load capacity and stiffness, and vice versa. The motor discussed in this report has a $2.525\times10^{-2}$-m- (1-in.-) long stator. The rotor has a $2.525\times10^{-2}$-m- (1-in.-) long hybrid segment comprising a $5.883\times10^{-3}$-m- (0.233-in.-) long section of circular laminations for levitation and a $1.937\times10^{-2}$-m- (0.767-in.-) long portion having six salient poles for rotation.

This report focuses exclusively on the nonrotating magnetic bearing action forces and static torque in a novel (8/6) hybrid motor. Three types of magnetic force measurements were made in which two diametrically opposed rotor poles were aligned with stator poles. In the first measurement, only one stator pole was energized, and the force on the centered rotor was recorded as a function of current. In this situation, the flux through the excited pole returns through a number of unexcited poles. In the second type of measurement, a proportional-derivative (PD) algorithm was used to levitate the nonrotating rotor. The rotor was then vertically displaced using a fixture containing a load cell, and the stator coil currents and force exerted on the rotor were recorded for each displacement value. In the corresponding analysis, the measured currents were utilized directly, thus making the calculations independent of the control law. The third measurement was the determination of static torque for rotor angles ranging from alignment to 30° from alignment. The question to answer is, "can one successfully apply one-dimensional magnetic field analysis to the complex three-dimensional hybrid rotor to obtain the associated electromagnetic radial forces?"

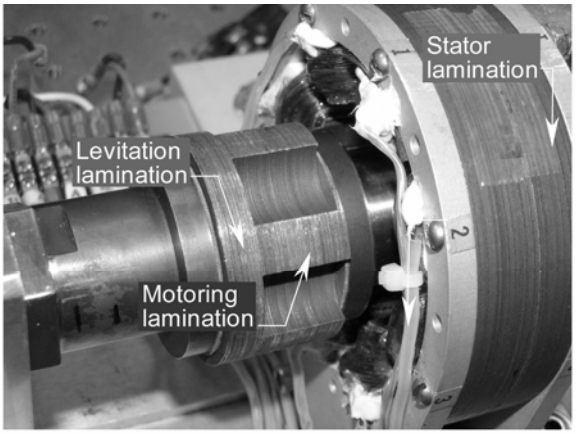


Figure 1.—Disassembled eight-pole stator and six-pole hybrid rotor of magnetic-bearing switched-reluctance motor (MBSRM).

A list of symbols used in this report is given in the appendix to aid the reader.

## Derivation of General Magnetic Force Equation

Figures 2 and 3 depict a portion of the rotor and a portion of a stator tooth on which the stator coil is energized to produce a magnetic field flux density $B$. The magnetic field interacts with the rotor at a distance $g$. The magnetic energy $w$ is given by the volume integral equation

$$w = \frac{1}{2\mu_0}\iiint B^2 \mathrm{d}V \tag{1}$$

where $\mu_0$ is the permeability of free space. Integration over only the flux volume $V$ is possible if the magnetic core material is operating within its linear range so that the energy stored in the core can be neglected compared with that in the gap. Referring to figure 2, it can be shown from equation (1) that the magnetic radial force on the rotor toward the stator is

$$F = -\frac{\mathrm{d}w}{\mathrm{d}g} = -\frac{B^2}{2\mu_0} L^c l_{tw} = -EA \tag{2}$$

where d$g$ is the differential gap length, $L^c$ is the stack length of the circular laminations, $l_{tw}$ is the width of a stator tooth, $E$ is the general energy density between a stator pole and the rotor, and $A$ is the general common cross-sectional area between a stator pole and the rotor surface. Similarly, the instantaneous torque on the rotor (fig. 3) at the scalloped segment is given by

$$T = -\frac{\mathrm{d}w}{\mathrm{d}\theta} = \begin{cases} -\dfrac{B^2}{2\mu_0} L^s g r & \text{partial overlap} \\ 0 & \text{aligned, no overlap} \end{cases} \tag{3}$$

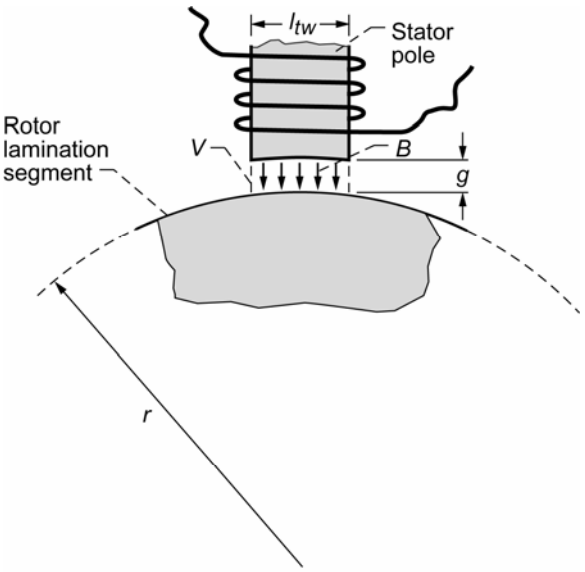


Figure 2.—Side view of circular rotor and stator tooth segment of 8/6 MBSRM, where $B$ is magnetic flux density, $g$ is gap length, $l_{tw}$ is tooth width, $r$ is outer radius of rotor laminations, and $V$ is flux volume.

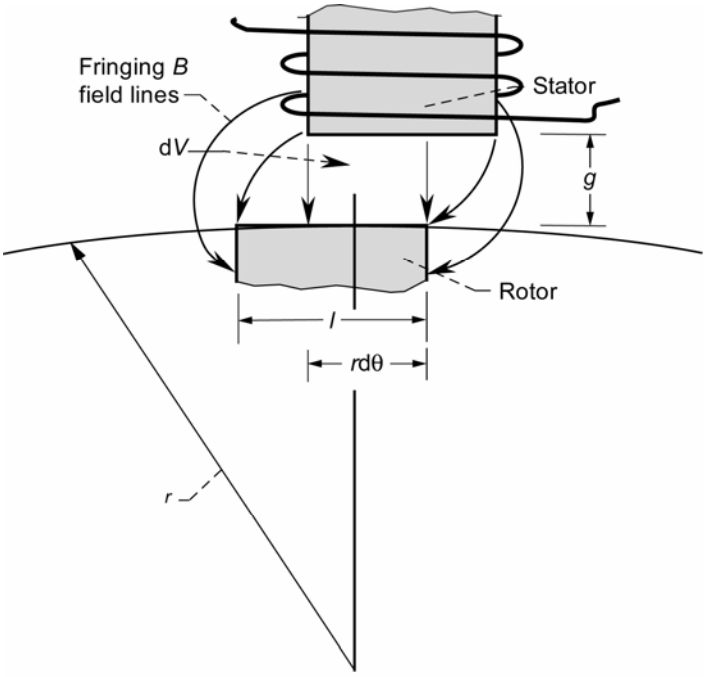


Figure 3.—Side view sketch of scalloped rotor-stator tooth segment, where $g$ is gap length, $l$ is rotor tooth width, $r$ is outer radius of rotor laminations, and $dV$ is differential flux volume.

where dθ is the differential angular displacement, $L^s$ is the stack length of the scalloped laminations, $g$ is the gap length, and $r$ is the outer radius of scalloped lamination section of the rotor. The mathematical form and value of the radial $B$ field impinging on the nonrotating asymmetric rotor will be determined next.

## Nonlevitated Magnetic Equivalent Circuit Modeling for Centered Rotor

Figure 4 is an axial view of the motor.

### Circular Lamination Force Contribution

A complex three-dimensional magnetic field topology exists in and around the rotor because of its hybrid design. However, the analysis will be restricted to a one-dimensional approach in order to reduce the mathematical complexity of the static radial force derivation. Each rotor segment (circular lamination stack and scalloped lamination stack) will be treated as an independent entity, and accordingly, we develop a one-dimensional magnetic radial force description for each rotor segment. The magnetic radial forces will then be summed to obtain the total static magnetic radial force on the rotor.

Figure 5 depicts the equivalent two-dimensional flux distribution in the rotor's circular laminations and the eight stator poles. Each stator pole is at a distance $g_0$ (gap length) from the circular lamination stack and each pole shares a common cross-sectional area $A^c$ with the circular laminations. Figure 6 is the corresponding magnetic equivalent circuit of figure 5. Both figures will be employed in deriving the static magnetic radial force equations.

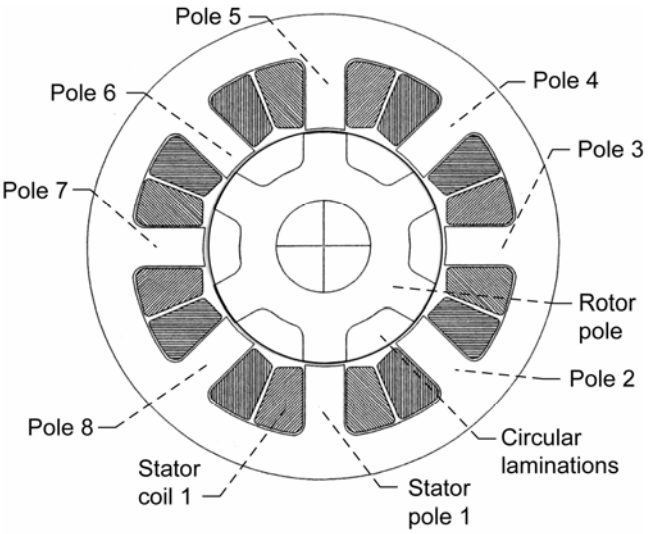


Figure 4.—Axial view of the 8/6 hybrid MBSRM with rotor and stator pole 1 aligned.

The common cross-sectional area $A^c$ between the circular lamination stack and each stator pole can be expressed as

$$A_k^c = A^c, \quad k = 1...8 \tag{4}$$

where $A^c = L^c l_{tw}$. The flux at stator pole 1 $\phi_1^c$, produced by energizing coil 1, is distributed equally among the other seven poles. The flux distribution obeys the relation

$$\phi_1^c = \sum_{k=2}^{8} \phi_k^c \tag{5}$$

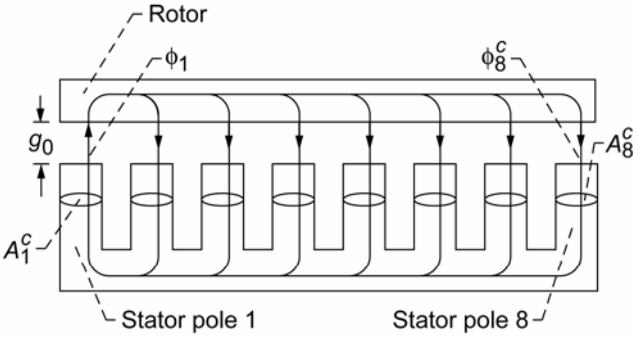


Figure 5.—Equivalent two-dimensional rotor-stator flux distribution for nonlevitated 8/6 hybrid MBSRM, where for the circular lamination $\phi_k^c$ is magnetic flux between stator pole $k$ and rotor lamination stack, $A_k^c$ is cross-sectional area between stator pole $k$ and rotor lamination stack, and $g_0$ is gap length.

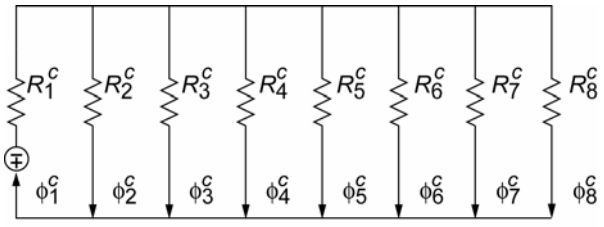


Figure 6.—Magnetic equivalent circuit for nonlevitated 8/6 hybrid MBSRM, where for circular lamination $R_k^c$ is reluctance and $\phi_k^c$ is magnetic flux between stator pole $k$ and rotor lamination stack.

and for a rotor that is radially centered, the reluctances between the stator poles $k$ and the rotor are related by

$$R_k^c = R_{k+1}^c, \quad k = 1...7 \tag{6}$$

The total reluctance for the flux passing through the powered pole is

$$R_T^c = R_1^c + R_{\|}^c \tag{7}$$

where $R_1^c$ is in series with the parallel reluctances $R_2^c, R_3^c, R_4^c, R_5^c, R_6^c, R_7^c$, and $R_8^c$. Further, it can be shown that equation (7) has the form

$$R_T^c = \frac{8}{7}\left(\frac{g_0}{\mu_0 A^c}\right) \tag{8}$$

From the basic magnetic circuit equation, the magnetomotive force

$$mmf = \phi R \tag{9}$$

and noting that $mmf = ni$, where $n$ is the number of turns in the coil and $i$ is the current in the coil, we can write the flux expression

$$\phi_1^c = \frac{ni}{R_T^c} \tag{10}$$

Substituting equation (8) into (10) yields

$$\phi_1^c = \frac{7}{8}\left(\frac{\mu_0 A^c ni}{g_0}\right) \tag{11}$$

from which we obtain the flux density at pole 1:

$$B_1^c = \frac{\phi_1^c}{A^c} = \frac{7}{8}\left(\frac{\mu_0 ni}{g_0}\right) \tag{12}$$

Substituting equation (12) into an expression similar to equation (2), we can write the magnetic radial force as

$$F_1^c = \frac{1}{2}\left(\frac{49}{64}\right)\left(\frac{A^c}{\mu_0}\right)\left(\frac{\mu_0^2 n^2 i^2}{g_0^2}\right) \tag{13}$$

where the $B$ field is considered uniform. Equation (13) is the static magnetic radial force due to pole 1 (fig. 4). The oppositely directed radial forces produced by poles 3 and 7 will sum to zero. Likewise, the resultant magnetic force produced by poles 2, 4, 6, and 8 is zero. Hence, only the radial force at pole 5 will contribute to the resultant force on the rotor. Because of the flux symmetry in the rotor and stator, we can write the magnetic field at pole 5 as

$$B_5^c = \frac{1}{7} B_1^c \tag{14}$$

and substituting equation (12) into (14) yields

$$B_5^c = \frac{1}{8}\left(\frac{\mu_0 ni}{g_0}\right) \tag{15}$$

The magnetic radial force at pole 5 can now be written as

$$F_5^c = \frac{1}{2}\left(\frac{1}{64}\right)\left(\frac{A^c}{\mu_0}\right)\left(\frac{\mu_0^2 n^2 i^2}{g_0^2}\right) \tag{16}$$

and the net downward magnetic force produced by poles 1 and 5 on the circular laminations is given as

$$F_{net}^c = F_1^c - F_5^c \tag{17}$$

Substituting equations (13) and (16) into (17) yields the net downward magnetic force on the circular lamination stack;

$$F_{net}^{c} = \frac{3}{8}\left(\frac{A^{c}\mu_0 n^2}{{g_0}^2}\right) i^2 \tag{18}$$

Substituting the actual value of the constants gives

$$F_{net}^{c} = 5.037\, i^2 \tag{19}$$

We now determine the static magnetic radial force on the scalloped laminations by employing some aspects of the previous discussion.

## Scalloped Lamination Force Contribution

Figure 7 depicts the equivalent two-dimensional flux distribution in the rotor scalloped laminations and their adjacent stator poles. Each rotor pole is at a nominal distance $g_0$ from its adjacent stator poles. Four stator poles—2, 4, 6, and 8 (figs. 4 and 7)—share a common cross-sectional area $\frac{1}{3}A^s$ with four adjacent rotor poles. Figure 8 is the corresponding magnetic equivalent circuit of figure 7. Additionally, in the spirit of rough approximation, we neglect any fringing effects from the rotor to stator poles 3 and 7. The expected large reluctance between the stator poles and the scalloped cavities will result in a relatively small return flux. However, in later sections analyzing the unaligned centered rotor and the aligned levitated rotor, the fringing effect will be included to give a more complete description of the levitation force on the rotor.

Observation of figure 4 reveals that only the stator poles labeled as 1, 2, 4, 5, 6, and 8 provide significant paths for the circulating magnetic flux, and each pole 2, 4, 6, and 8 has an equivalent, effective common stator-rotor area that is one-third that of stator pole 1 or 5. The common cross-sectional area between the rotor scalloped lamination stack and a stator pole can be expressed as

$$A_1^s = A_5^s = A^s \tag{20}$$

and

$$A_{2k}^s = \tfrac{1}{3}A_1^s = \tfrac{1}{3}A^s, \quad k = 1...4 \tag{21}$$

The reluctance between the rotor and stator poles for the radially centered rotor is hence given as

$$R_1^s = \frac{g_0}{\mu_0 A_1^s},\ R_2^s = \frac{g_0}{\mu_0 \frac{A_1^s}{3}} = \frac{3g_0}{\mu_0 A_1^s} = 3R_1^s \tag{22}$$

and

$$R_1^s = R_5^s \quad \text{and} \quad R_{2k}^s = R_2^s, \quad k = 2...4 \tag{23}$$

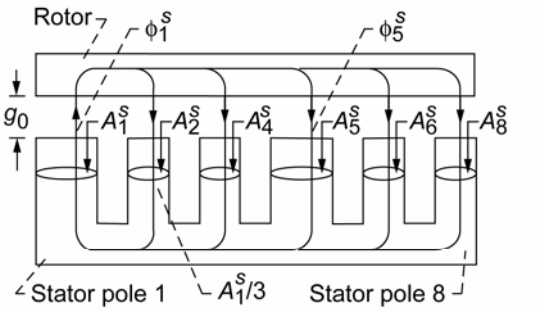


Figure 7.—Equivalent two-dimensional rotor-stator flux distribution for nonlevitated 8/6 hybrid MBSRM, where for scalloped lamination $g_0$ is gap length, $\phi_k^s$ is magnetic flux between stator pole $k$ and rotor lamination stack, and $A_k^s$ is cross-sectional area between stator pole $k$ and rotor lamination stack.

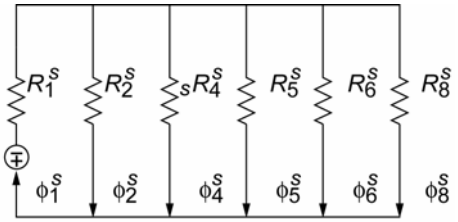


Figure 8.—Magnetic equivalent circuit for nonlevitated 8/6 hybrid MBSRM, where for scalloped lamination $R_k^c$ is reluctance and $\phi_k^c$ is magnetic flux between stator pole $k$ and rotor lamination stack.

The total reluctance in the magnetic circuit can be written as

$$R_T^s = R_1^s + R_{\|}^s \tag{24}$$

where $R_1^s$ is in series with the parallel reluctances $R_2^s, R_4^s, R_5^s, R_6^s$, and $R_8^s$. The resultant parallel reluctance is thus obtained by

$$R_{\|}^s = \frac{1}{\left(\frac{1}{R_5^s} + \sum_{k=1}^{4}\frac{1}{R_{2k}^s}\right)} \tag{25}$$

Substituting equation (25) into (24) and using equations (22) and (23), it can be shown that the total reluctance at pole 1 is

$$R_T^s = \frac{10}{7}\left(\frac{g_0}{\mu_0 A_1^s}\right) \tag{26}$$

Using the magnetomotive force argument, we can derive equation (27)

$$\phi_1^s = \frac{7}{10}\left(\frac{\mu_0 \mathrm{A}_1^s ni}{\mathrm{g}_0}\right) \tag{27}$$

The flux density extant at pole 1 and its adjacent salient rotor pole is thus given as

$$B_1^s = \frac{\phi_1^s}{A_1^s} = \frac{7}{10}\left(\frac{\mu_0 ni}{g_0}\right) \tag{28}$$

Substituting equation (28) into an expression similar to equation (2), the magnetic force at pole 1 is given as

$$F_1^s = \frac{1}{2}\left(\frac{49}{100}\right)\left(\frac{A_1^s}{\mu_0}\right)\left(\frac{\mu_0^2 n^2 i^2}{g_0^2}\right) \tag{29}$$

Equation (29) represents the magnetic force, due to stator pole 1, on the aligned salient pole of the rotor. The resultant magnetic force on the rotor, produced by poles 2 and 8, cancels the resultant magnetic force produced by poles 4 and 6. Hence, only the magnetic force at pole 5 will contribute to the resultant force on the rotor. The flux at pole 5 can be expressed as

$$\phi_5^s = \phi_1^s - \sum_{k=1}^{4} \phi_{2k}^s \tag{30}$$

The flux relation at the poles can be written as

$$\phi_{2k}^s = \phi_2^s, \quad k = 2...4 \tag{31}$$

and making the appropriate substitutions it can be shown that

$$\phi_5^s = \frac{3}{10}\left(\frac{\mu_0 A_5^s ni}{g_0}\right) \tag{32}$$

Using equation (32), the magnetic force between pole 5 and its adjacent salient rotor pole is

$$F_5^s = \frac{1}{2}\left(\frac{9}{100}\right)\left(\frac{A_5^s}{\mu_0}\right)\left(\frac{\mu_0^2 n^2 i^2}{g_0^2}\right) \tag{33}$$

The net downward magnetic force produced by poles 1 and 5 on their corresponding salient rotor poles is

$$F_{net}^s = F_1^s - F_5^s \tag{34}$$

Substituting equations (29) and (33) into (34) yields the force expression

$$F_{net}^s = \frac{1}{5}\left(\frac{A^s \mu_0 n^2}{g_0^2}\right) i^2 \tag{35}$$

where $A^s = L^s l_{tw}$. Equation (35) represents the net downward magnetic force on the scalloped lamination stack. Substituting the actual values of the constants gives

$$F_{net}^s = 8.845\, i^2 \tag{36}$$

The total net downward magnetic force on the centered nonlevitated hybrid rotor is the sum of the net downward magnetic force on the circular lamination stack and the net downward magnetic force on the scalloped lamination stack:

$$F_{t(net)} = F_{net}^c + F_{net}^s \tag{37}$$

Substituting equations (19) and (36) into (37) yields

$$F_{t(net)} = 13.88\, i^2 \tag{38}$$

The fraction of force contributed by the circular lamination segment is

$$\frac{F_{net}^c}{F_{t(net)}} = \frac{5.037\, i^2}{13.88\, i^2} \simeq 0.36 = 36\,\text{percent} \tag{39}$$

and the fraction by the scalloped segment is

$$\frac{F_{net}^s}{F_{t(net)}} = \frac{8.845\, i^2}{13.88\, i^2} \simeq 0.64 = 64\,\text{percent} \tag{40}$$

The circular lamination stack experiences approximately 36 percent of the total net downward magnetic force, while the scalloped lamination experience approximately 64 percent of said force. The relative stack lengths of the circular and scalloped laminations are $L^c$ = 0.23 and $L^s$ = 0.77, respectively. Note that the forces in equations (39) and (40) are not proportional to the stack lengths. This discrepancy is due to the differences in return paths of the flux in the hybrid rotor. The following section outlines the experimental procedure for obtaining the nonlevitated magnetic radial force on the rotor.

## Experimental Centered-Force Procedure

The experimental nonlevitated magnetic radial force on the rotor was obtained by mounting the rotor between two load cells (see fig. 9) while ensuring that the rotor's axis was radially centered in the stator. A salient rotor pole was aligned with stator pole 1 (see fig. 4). The preload voltages of the cells were then zeroed to eliminate the preload weight from the data. Stator pole 1 was energized, and the resulting magnetic force on the rotor produced a larger reading on the lower cell and a smaller reading on the upper cell. The difference in the readings gave the net force on the rotor. This procedure was repeated for several values of coil current ranging from 0.982 to 2.027 A. The procedure was repeated with pole 5 as the sole energized pole.

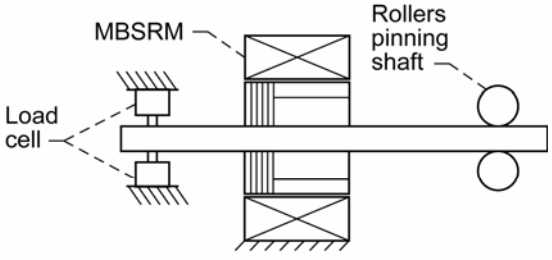


Figure 9.—Experimental setup used in obtaining nonlevitation magnetic radial forces for 8/6 hybrid MBSRM.

## Experimental and Theoretical Centered-Force Comparison

The experimental and theoretical magnetic radial force data plot are presented in figure 10. Because of flux leakage and field fringing effects at the stator and rotor pole edges, uncertainties in geometry, rotor-stator alignment, and material properties, we must apply a derating factor to equation (38). Reference 9 presents a detailed treatment of the derating factor, wherein a factor of 0.88 was determined for one particular active magnetic bearing. In contrast, a graph in reference 10 shows a derating factor of 0.6 for our gap $g_0$ ($5\times10^{-4}$ m). For this hybrid rotor configuration, which clearly is different from that of a pure magnetic bearing, a derating of 0.87 gives the closest agreement with the experimental results (see eq. (41) and fig. 10):

$$F_{t(net)} = (13.88\times 0.87)\, i^2 \tag{41}$$

Figure 10 depicts the experimental least-squares-fit magnetic force curves for the upper and lower poles, and the theoretical magnetic force curve. In the following section, the nonlevitated unaligned rotor-stator radial force equations are derived for the hybrid rotor.

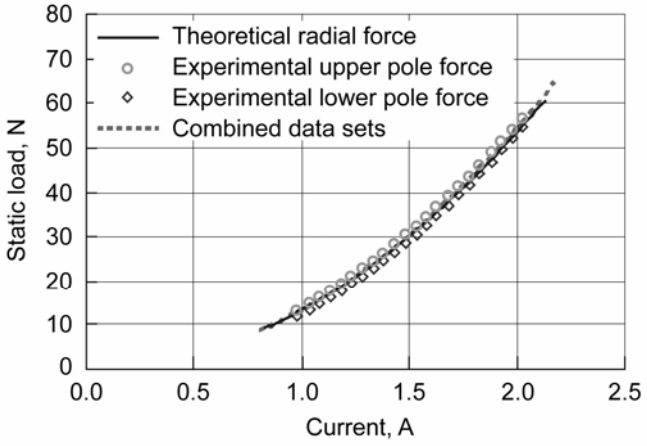


Figure 10.—Nonlevitation magnetic radial force curves for 8/6 hybrid MBSRM. Experimental least-squares-fit curves (dotted lines) for upper and lower poles and theoretical curve (solid line).

## Nonlevitated Unaligned Rotor Analysis

The analysis presented in previous sections clearly demonstrates that one can make a reasonably accurate prediction of electromagnet forces on a radially centered hybrid rotor using two-dimensional visualization and one-dimensional electromagnetic force analysis. With this fact established, we will estimate, without experimental verification, the radial force on the unaligned radially centered rotor, that is, a rotor that is rotated so that the motoring section has an unfavorable misalignment with the powered stator pole 1, as depicted in figure 11. Using a force symmetry argument similar to that presented in earlier sections, it can be shown that only poles 1 and 5 are relevant in determining the net force on the hybrid rotor. The analysis begins by approximating the reluctance between pole 1 or 5 and the adjacent scallop cavities:

$$R_1^s = \frac{g_a}{\mu_0 A_a} = R_5^s \tag{42}$$

where $g_a = \left(\frac{g_b + g_c}{2}\right)$ is the average stator-rotor gap length at stator pole 1 or 5 (fig. 11), $g_b$ is the distance between a corner edge of the salient stator pole 1 or 5 and either of its adjacent salient rotor pole corner edges, and $g_c$ is the gap length between the midpoint of either pole face and the base of its adjacent scallop cavity. Here, $A_a = \left(\frac{A_b^s + A_c^s}{2}\right)$ is the average of the stator pole face area $A_b^s$ and its adjacent scallop cavity area $A_c^s$. The face area of pole 1 is

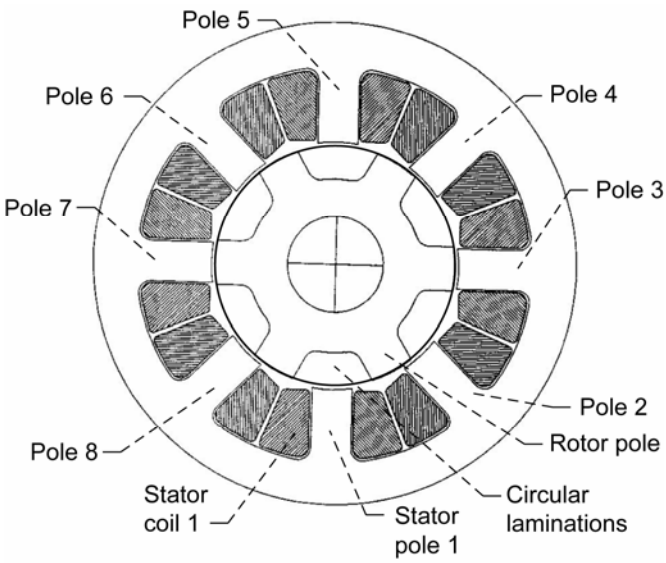


Figure 11.—Axial view of 8/6 hybrid MBSRM with rotor and stator pole 1 unaligned.

$A_b^s = A^s = 2\times10^{-4}$ m$^2$, and the surface area inside a scallop cavity was determined to be $A_c^s = 4.35\times10^{-4}$ m$^2$. Substituting these values into the average stator-rotor gap length and area expressions result in $g_a = 6.25\times10^{-3}$ m and $A_a = 3.17\times10^{-4}$ m$^2$. We can rewrite $A_a$ in terms of $A^s$:

$$A_a = 1.59A^s \tag{43}$$

and $g_a$ in terms of $g_0$:

$$g_a = 12.5g_0 \tag{44}$$

It can be shown by substituting equations (43) and (44) into (42) that

$$R_1^s = R_5^s = 7.86R_0^s = 1.57\times10^7 \text{ H}^{-1} \tag{45}$$

where $R_0^s$ is the nominal reluctance at the aligned scalloped segment. Here, the estimated reluctance at the unaligned pole is almost eight times that of an aligned pole. Note that this value of the reluctance applies to both poles 1 and 5. The remaining pole reluctances are

$$R_k^s = \frac{g_0}{\mu_0 A_k^s}, \quad k = 2...4, 6...8 \tag{46}$$

We know that

$$A_3^s = A_7^s = A^s \tag{47}$$

hence

$$R_3^s = R_7^s = R_0^s \tag{48}$$

then

$$R_2^s = \frac{g_0}{\mu_0\left(\frac{A^s}{3}\right)} = \frac{3g_0}{\mu_0 A^s} = 3R_0^s \tag{49}$$

where $R_{2k}^s = R_2^s, \quad k = 2...4$. The total parallel reluctance due to poles 2, 3, 4, 5, 6, 7, and 8 is given as

$$R_{\|}^s = \frac{1}{\left(\frac{4}{R_2^s} + \frac{2}{R_3^s} + \frac{1}{R_5^s}\right)} \tag{50}$$

and substituting equations (45), (48), and (49) into (50) gives

$$R_{\|}^s = 0.29R_0^s \tag{51}$$

Hence, the total reluctance of the magnetic circuit through pole 1 is

$$R_{T1}^s = R_1^s + R_{\|}^s = 7.86R_0^s + 0.29R_0^s = 8.15R_0^s \tag{52}$$

The reluctance value derived in equation (52) is used later in estimating the levitation load on the rotor. Substituting $R_0^s = \frac{g_0}{\mu_0 A^s} = 1.99\times10^6 \text{ H}^{-1}$ into equation (52) gives $R_{T1}^s = 1.63\times10^7 \text{ H}^{-1}$. The total flux at pole 1 has the form

$$\phi_1^s = \frac{ni}{R_{T1}^s} = \left(6.15\times10^{-8} \text{ H}\right)ni \tag{53}$$

from which we can determine the flux density:

$$B_1^s = \frac{\phi_1^s}{A^s} = \left(\frac{6.15\times10^{-8} \text{ H}}{2\times10^{-4} \text{ m}^2}\right)ni = \left(6.63\times10^{-2} \text{ H/m}^2\right)i \tag{54}$$

Using equation (2), the radial force at pole 1 is thus

$$F_1^s = \frac{1}{2}\left(\frac{A^s}{\mu_0}\right)\left(B_1^s\right)^2 = 0.35i^2 \tag{55}$$

The next task is to determine the flux fraction at pole 5, which will allow computation of the magnetic force at pole 5. The difference between this force and the force at pole 1 will give the net magnetic force on the unaligned hybrid rotor.

The fraction of the total flux passing through pole 5 is determined by its reluctance ratio, the combined parallel reluctance of all the return poles divided by the reluctance of pole 5:

$$R_{5\_ratio}^s = \frac{R_{\|}^s}{R_5^s} = \frac{0.29R_0^s}{7.86R_0^s} \simeq 0.037 \tag{56}$$

The flux at pole 5 is now obtained by employing equation (53):

$$\phi_5^s = R_{5\_ratio}^s \phi_1^s = 0.037 \times \frac{ni}{R_{T1}^s} \tag{57}$$

or simply

$$\phi_5^s = 4.86\times10^{-7} i \tag{58}$$

The magnetic radial force at pole 5 is

$$F_5^s = \frac{\left(\phi_5^s\right)^2}{2\mu_0 A^s} = 4.71\times10^{-4} i^2 \tag{59}$$

The net downward magnetic radial force on the unaligned scalloped section of the rotor due to poles 1 and 5 is

$$F_{u\_net}^s = F_1^s - F_5^s \tag{60}$$

Substituting equations (55) and (59) into (60) produces

$$F_{u\_net}^s \simeq 0.35i^2 \tag{61}$$

The ratio of the net downward magnetic force on the unaligned scalloped stack to that on the aligned scalloped stack $F_{net}^s$ is

$$\frac{F_{u\_net}^s}{F_{net}^s} = \frac{0.35i^2}{8.85i^2} \simeq 0.039 = 3.9 \text{ percent} \tag{62}$$

Note that the unaligned scallop magnetic force load is only 3.9 percent of the magnetic force load produced by the aligned scallop. This is a reasonable result, considering the large reluctances of the scallop cavities located at poles 1 and 5. Taking into account the contributions of the circular laminations, the total net downward magnetic radial force on the unaligned rotor is

$$F_{t(u\_net)} = F_{net}^c + F_{u\_net}^s \tag{63}$$

We know from equations (19) and (36) that the aligned net radial force on the circular laminations and scallops are $F_{net}^{c} \simeq 5.037 i^2$ and $F_{net}^{s} \simeq 8.845\, i^2$, respectively, from which the total net downward magnetic force on the aligned rotor is

$$F_{t(net)} = F_{net}^{c} + F_{net}^{s} \tag{64}$$

The ratio of the total net downwards magnetic force of the unaligned rotor to the total net downwards magnetic force on the aligned rotor is

$$\frac{F_{t(u\_net)}}{F_{t(net)}} = \frac{(5.037 + 0.348)i^2}{(5.037 + 8.845)i^2} \simeq 0.39 = 39\,\text{percent} \tag{65}$$

Equations (62) and (65) highlight the importance of the circular lamination stack in this hybrid motor; that is, the load capacity in the unaligned orientation is substantially enhanced by the circular lamination segment (this is critical for maintaining rotor stability during the motoring operation). In subsequent sections, the general levitation force equations are derived for the hybrid rotor that is displaced vertically from its radially centered position within the stator.

# Levitation Magnetic Equivalent Circuit Modeling

The analysis begins by employing the magnetic equivalent circuit depicted in figure 12, which relates to the magnetically levitated state of the nonrotating, aligned, vertically displaced hybrid rotor. The rotor was magnetically levitated using stator poles 1, 3, 5, and 7 (fig. 4).

### Levitation Flux Derivation

We designate the coil currents as $i_1$, $i_3$, $i_5$, and $i_7$ for the respective stator poles 1, 3, 5, and 7. Each coil has $n$ turns. These currents generate the magnetic fluxes $\phi_1$, $\phi_3$, $\phi_5$, $\phi_7$, $\phi_{2,8}$, and $\phi_{4,6}$, where $\phi_{2,8}$ and $\phi_{4,6}$ represent the return fluxes due to pole pairs (2 and 8) and (4 and 6) on either side of poles 1 and 5, respectively. Because multiple poles were energized during levitation, we will use the permeance expression instead of the reluctance term in order to facilitate easy mathematical manipulation; hence, by referencing figure 12, equations (66a) to (66e) are written by applying the magnetic circuit equation to various closed paths (all of which go through pole 1, which has a permeance $P_1$):

$$\frac{\phi_3}{P_3} - ni_3 = \frac{\phi_1}{P_1} + ni_1 \tag{66a}$$

$$\frac{\phi_5}{P_5} + ni_5 = \frac{\phi_1}{P_1} + ni_1 \tag{66b}$$

$$\frac{\phi_7}{P_7} - ni_7 = \frac{\phi_1}{P_1} + ni_1 \tag{66c}$$

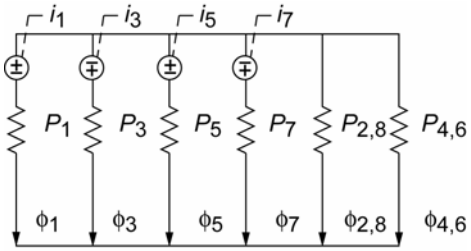


Figure 12.—Magnetic equivalent circuit for levitated 8/6 hybrid MBSRM, where $i_k$ is current in coil $k$, $P_k$ is permanence at stator pole $k$, and $\phi_k$ is magnetic flux at stator pole $k$.

$$\frac{\phi_{2,8}}{P_{2,8}} = \frac{\phi_1}{P_1} + ni_1 \tag{66d}$$

$$\frac{\phi_{4,6}}{P_{4,6}} = \frac{\phi_1}{P_1} + ni_1 \tag{66e}$$

Conservation of the magnetic flux assures that the sum of the magnetic fluxes is equal to zero, hence

$$\phi_1 + \phi_3 + \phi_5 + \phi_7 + \phi_{2,8} + \phi_{4,6} = 0 \tag{66f}$$

The solution of equations (66a) to (66f) is given by

$$\phi_1 = -\frac{P_1}{P_T}\Big[P_3 i_3 - P_5 i_5 + P_7 i_7 + (P_3 + P_5 + P_7 + P_{2,8} + P_{4,6}) i_1\Big] n \tag{67a}$$

$$\phi_3 = \frac{P_3}{P_T}\Big[P_1 i_1 + P_5 i_5 - P_7 i_7 + (P_1 + P_5 + P_7 + P_{2,8} + P_{4,6}) i_3\Big] n \tag{67b}$$

$$\phi_5 = -\frac{P_5}{P_T}\Big[P_3 i_3 - P_1 i_1 + P_7 i_7 + (P_1 + P_3 + P_7 + P_{2,8} + P_{4,6}) i_5\Big] n \tag{67c}$$

$$\phi_7 = \frac{P_7}{P_T}\Big[P_1 i_1 - P_3 i_3 + P_5 i_5 + (P_1 + P_3 + P_5 + P_{2,8} + P_{4,6}) i_7\Big] n \tag{67d}$$

$$\phi_{2,8} = \frac{P_{2,8}}{P_T}\Big[P_1 i_1 - P_3 i_3 + P_5 i_5 - P_7 i_7\Big] n \tag{67e}$$

$$\phi_{4,6} = \frac{P_{4,6}}{P_T}\Big[P_1 i_1 - P_3 i_3 + P_5 i_5 - P_7 i_7\Big] n \tag{67f}$$

where for notational convenience we define the sum of permeances as

$$P_T \equiv P_1 + P_3 + P_5 + P_7 + P_{2,8} + P_{4,6} \tag{67g}$$

Equations (67a), (67c), (67e), (67f), and (67g) are used to derive the electromagnetic levitation force equations for the rotor displaced vertically inside the stator. In subsequent sections, separate magnetic force equations for the circular and scalloped lamination segments are derived.

## Levitation Force on the Circular Laminations

The common cross-sectional area between the circular laminations and pole 1 or 5 is given as $A^c = L^c l_{tw}$. The rotor's vertical displacement $x$ from its nominal position affects the gap lengths $g_k$, hence

$$g_1 = g_0 + x \tag{68}$$

at stator pole 1, and

$$g_5 = g_0 - x \tag{69}$$

at stator pole 5. In addition, the gaps at the return flux poles 2 and 8 can be written as

$$g_{2,8} = g_0 + x\cos(45°) \tag{70}$$

and for poles 4 and 6

$$g_{4,6} = g_0 - x\cos(45°) \tag{71}$$

where 45° is the angle between adjacent stator poles. The approximate permeances between the poles and the circular lamination stack are

$$P_3^c = P_7^c = P_0^c = \frac{\mu_0 A^c}{g_0} \tag{72}$$

$$P_k^c = \frac{\mu_0 A^c}{g_k}, \quad k = 1,5; \quad P_{2,8}^c = \frac{2\mu_0 A^c}{g_{2,8}}; \quad \text{and } P_{4,6}^c = \frac{2\mu_0 A^c}{g_{4,6}}. \tag{73}$$

For the circular laminations, equations (67c) and (67g) are utilized to obtain the flux at pole 5, thus

$$\phi_5^c = -\frac{P_5^c}{P_T^c}\Big[ P_3^c i_3 - P_1^c i_1 + P_7^c i_7 + \left( P_1^c + P_3^c + P_7^c + P_{2,8}^c + P_{4,6}^c \right) i_5 \Big] n \tag{74}$$

The equations for the magnetic field and energy density at pole 5 are, respectively,

$$B_5^c(x) = \frac{\phi_5^c(x)}{A^c} \tag{75a}$$

$$E_5^c(x) = \frac{[B_5^c(x)]^2}{2\mu_0} \tag{75b}$$

The magnetic force on the rotor due to pole 5 is then obtained by employing equation (2), hence

$$F_5^c = -E_5^c(x) A^c \tag{76}$$

where $B$ is considered uniform. Using equation (67f), the return magnetic flux equation for poles 4 and 6 is

$$\phi_{4,6}^c = \frac{P_{4,6}^c}{P_T^c}\left( P_1^c i_1 - P_3^c i_3 + P_5^c i_5 - P_7^c i_7 \right) n \tag{77}$$

where $P_T^c$ is the sum of permeances at the circular laminations. The equations for the magnetic field and energy density at poles 4 and 6 are, respectively,

$$B_{4,6}^c(x) = \frac{\phi_{4,6}^c(x)}{A^c} \tag{78a}$$

$$E_{4,6}^c(x) = \frac{\left[ B_{4,6}^c(x) \right]^2}{2\mu_0} \tag{78b}$$

and the magnetic force due to poles 4 and 6 is

$$F_{4,6}^c = -E_{4,6}^c(x) 2A^c \tag{79}$$

The total magnetic force due to pole 5 and its adjacent poles 4 and 6 is thus

$$F_{T\,(upper)}^c = F_5^c + F_{4,6}^c \tag{80}$$

Similarly, we can calculate the net downward magnetic force created by poles 1, 2, and 8. The magnetic force at pole 1 is

$$F_1^c = -E_1^c(x) A^c \tag{81}$$

and the magnetic force due to the return flux poles 2 and 8 is

$$F_{2,8}^c = -E_{2,8}^c(x) 2A^c \tag{82}$$

The total magnetic force due to pole 1 and its adjacent poles 2 and 8 is thus

$$F_{T\,(lower)}^c = F_1^c + F_{2,8}^c \tag{83}$$

The net magnetic levitation force on the circular laminations, due to poles 1, 2, 4, 5, 6, and 8 can now be written:

$$F_{T(net\_lev)}^c = F_{T\,(upper)}^c + F_{T\,(lower)}^c \tag{84}$$

Note that for the vertically displaced rotor, the net force on the circular lamination stack, due to poles 3 and 7, is identically zero.

## Levitation Force on the Scalloped Laminations

We now determine the net force on the scalloped laminations. The common cross-sectional area between the

scalloped laminations and pole 1 or 5 is given as $A^s = L^s l_{tw}$, where $L^s$ is the scalloped rotor lamination stack length. For the return poles 2 or 8 and 4 or 6, the common cross-sectional areas are $A^s_{(2,8)} = L^s l_{tw(2,8)}$ and $A^s_{(4,6)} = L^s l_{tw(4,6)}$ respectively, where the corresponding tooth widths are

$$l_{tw(2,8)} = \frac{1.03\times10^{-2}}{3} - x\sin(51.6°) \tag{85}$$

and

$$l_{tw(4,6)} = \frac{1.03\times10^{-2}}{3} + x\sin(51.6°) \tag{86}$$

Here, 51.6° is the angle between the midpoint of stator pole 1 and either of the midpoints of the overlap of its adjacent poles 2 or 8 with their adjacent rotor poles, and similarly for stator pole 5 and its adjacent poles 4 or 6. The approximate fringing permeance $P^s_3$ or $P^s_7$ at pole 3 or 7, respectively, is similar in value to that used in equation (53), hence

$$P^s_3 = P^s_7 = \frac{1}{R^s_{T1}} = 6.1509\times10^{-8}\ \text{H} \tag{87}$$

The remaining permeances are

$$P^s_k = \frac{\mu_0 A^s}{g_k},\quad k = 1,5;\quad P^s_{2,8} = \frac{2\mu_0 A^s_{2,8}}{g_{2,8}};\quad \text{and } P^s_{4,6} = \frac{2\mu_0 A^s_{4,6}}{g_{4,6}} \tag{88}$$

For the scalloped laminations, equations (67c) and (67g) are utilized to obtain the flux at pole 5, thus

$$\phi^s_5 = -\frac{P^s_5}{P^s_T}\Big[ P^s_3 i_3 - P^s_1 i_1 + P^s_7 i_7 + \left(P^s_1 + P^s_3 + P^s_7 + P^s_{2,8} + P^s_{4,6}\right) i_5 \Big] n \tag{89}$$

The equations for the magnetic field and energy density, at pole 5 are, respectively,

$$B^s_5 = \frac{\phi^s_5}{A^s} \tag{90a}$$

$$E^s_5(x) = \frac{[B^s_5(x)]^2}{2\mu_0} \tag{90b}$$

The magnetic force on the scalloped laminations, due to pole 5, is thus given as

$$F^s_5 = -E^s_5(x)A^s \tag{91}$$

Using equation (67f), the return magnetic flux equation for poles 4 and 6 is

$$\phi^s_{4,6} = \frac{P^s_{4,6}}{P^s_T}\left(P^s_1 i_1 - P^s_3 i_3 + P^s_5 i_5 - P^s_7 i_7\right) n \tag{92}$$

The equations for the magnetic field and energy density at poles 4 and 6 are, respectively,

$$B^s_{4,6} = \frac{\phi^s_{4,6}}{A^s_{4,6}} \tag{93a}$$

$$E^s_{4,6}(x) = \frac{[B^s_{4,6}(x)]^2}{2\mu_0} \tag{93b}$$

and the equation for the magnetic force due to poles 4 and 6 is now given as

$$F^s_{4,6} = -E^s_{4,6}(x)2A^s \tag{94}$$

where the gap expression for differentiation is $g_{4,6} = g_0 - x\cos(51.6°)$. 51.6° is the angle between the midpoint of stator pole 5 and either of the midpoints of the overlap of its adjacent poles 4 or 6 with their adjacent rotor pole. The equation for the total magnetic force due to pole 5 and its adjacent poles 4 and 6 on the scalloped laminations is thus

$$F^s_{T(upper)} = F^s_5 + F^s_{4,6} \tag{95}$$

Similarly, we can calculate the net magnetic force on the scallop laminations created by poles 1, 2, and 8. The magnetic force at pole 1 is

$$F^s_1 = -E^s_1(x)A^s \tag{96}$$

and the magnetic force due to the return flux poles 2 and 8 is

$$F^s_{2,8} = -E^s_{2,8}(x)2A^s \tag{97}$$

The total magnetic force due to pole 1 and its adjacent poles 2 and 8 is hence

$$F^s_{T(lower)} = F^s_1 + F^s_{2,8} \tag{98}$$

The net magnetic levitation force on the scalloped laminations due to poles 1, 2, 4, 5, 6, and 8 is thus

$$F^s_{T(net\_lev)} = F^s_{T(upper)} + F^s_{T(lower)} \tag{99}$$

Note that for the vertically displaced rotor, the net force on the scalloped lamination stack due to poles 3 and 7 is identically zero. The total net magnetic levitating force on the vertically displaced hybrid rotor can now be written:

$$F_{T(net\_lev)} = F^c_{T(net\_lev)} + F^s_{T(net\_lev)} \tag{100}$$

Clearly, the motor becomes a pure magnetic bearing if solid rings replace the scallops. In this instance equation (100) will

have only the $F^{c}_{T(net\_lev)}$ term, in which $A^{c}$ is replaced by a value that is representative of total face area of a stator pole. The experimental measurements and their comparisons with the predictions of equation (100) are presented in the following sections.

### Experimental Levitation Force Procedure

The experimental setup is similar to that displayed in figure 9 for the nonlevitated configuration, except that the rotor is constrained to move in the vertical plane only. The hybrid rotor was configured as shown in figure 4 and then magnetically levitated, without rotation, using stator poles 1, 3, 5, and 7 and a standard PD control law (see ref. 8). A vernier device supporting a load cell, which in turn is attached to the rotor via a wire, effects vertical motion. The rotor was then preloaded to ensure tension in the load cell for both positive and negative vertical displacements and the load cell voltage zeroed, thereby eliminating the combined preload and rotor weight from the data. Fifteen position data points, along with their four coil currents $i_1$, $i_2$, $i_3$, and $i_4$, were recorded.

### Experimental and Theoretical Levitation Force Comparison

The experimental rotor displacements discussed above along with their associated coil currents and the levitation force equations derived in (100) were programmed into Mathematica (Wolfram Research), which generated the predicted force data points.

Because of (1) flux leakage and field fringing effects at the stator and rotor pole edges, (2) experimental errors related to the forced rotor displacement, and (3) uncertainties in rotor-stator geometry, alignment, and material properties, a derating must be applied to the predicted data set. A derating of 0.72 gave the closest agreement to the experimental result. The absolute values of the experimental and derated theoretical data points were least squares fitted using Excel (Microsoft Corporation); both are presented in figure 13.

The static torque analysis for the hybrid rotor is discussed next.

## Torque Analysis

An algorithm that handles both the levitating and motoring functions controls the currents in the stator coils. Two pairs of opposing stator poles (at right angles to each other) levitate the rotor. The remaining two pairs of stator poles exert torque on the six-pole rotor lamination stack to produce rotation. Figure 14 is a plot of the experimental static torque obtained with the aid of a Magtrol dynamometer. Using equation (3), the predicted instantaneous torque, generated by two opposite stator poles during partial overlap, is given as

$$T = \left( \frac{\mu_0 n^2 L^s r}{g_0} \right) i^2 \qquad (101)$$

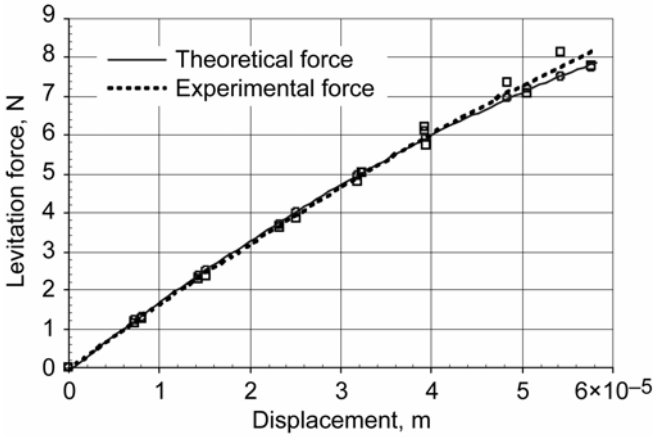


Figure 13.—Least-squares-fit experimental (dotted line) and theoretical (solid line) levitation magnetic radial force curves for 8/6 hybrid MBSRM.

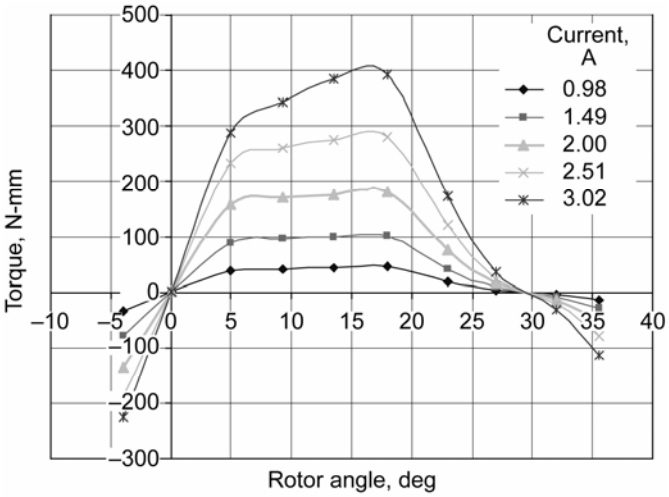


Figure 14.—Experimental torque graph for 8/6 hybrid MBSRM showing torque variation on rotor poles from –4° to 35.5°.

For a current of 2 A, the predicted instantaneous torque is 0.227 Nm. The average predicted torque is obtained by taking the product of the rotor theoretical duty cycle (22.5°/60°) and 0.227, which is 0.085 Nm. The average experimental torque, produced by the same 2 A current, is similarly obtained to be 0.058 Nm, using the experimental duty cycle (30°/60°). It is observed that the average experimental torque is approximately 0.68 times the average predicted torque. We surmise that this lower experimental average torque value may be due to significant fringing losses at the poles and the influence of the nearby circular laminations.

## Concluding Remarks

The nonrotating electromagnetic radial forces within a novel eight-stator-pole, six-rotor-pole magnetic-bearing switched-reluctance motor were examined theoretically and experimentally. The circular lamination stack and the scalloped lamination stack were treated as independent entities, and one-dimensional magnetic force equations were

developed for each. The total net magnetic forces on the rotor were obtained by summing the net magnetic forces on each segment and then applying derating factors of 0.87 for the nonlevitated case and 0.72 for the levitated case. These derating values are within the range of those discussed in previous studies.

The variation in the radial force derating factors is due, in part, to the disparate mode of operation; that is, forced displacement of the levitated rotor versus nonlevitation. Forced displacement of the levitated rotor introduces an additional source of error. A derating factor of 0.68 was determined for the average predicted torque.

In addition, it was demonstrated analytically that the load capacity of the hybrid rotor in the unaligned orientation is substantially enhanced by the presence of a circular lamination segment (this is critical for maintaining rotor stability during the motoring operation). Based on the analysis, we conclude that two-dimensional visualization and one-dimensional magnetic field analysis can be used for estimating, preliminarily, the electromagnetic levitation forces on the hybrid rotor with a derating factor of about 0.8 applied to the calculated force.

## References


1. Montague, Gerald, et al.: High-Temperature Switched-Reluctance Electric Motor. NASA Tech Briefs, vol. 27, no. 2, 2003.
2. Richter, E.; and Ferreira, C.: Performance Evaluation of a 250 kW Switched Reluctance Starter Generator. Conference Record of the 1995 IEEE Thirtieth IAS Annual Meeting, vol. 1, 1995, pp. 434–440.
3. MacMinn S.R.; and Jones, W.D.: A Very High Speed Switched-Reluctance Starter-Generator for Aircraft Engine Applications. Proceedings of the IEEE 1989 Aerospace and Electronics Conference, vol. 4, 1989, pp. 1758–1764.
4. Miller, T.J.E.: Faults and Unbalance Forces in the Switched Reluctance Machine. IEEE Trans. Ind. Applicat., vol. 31, issue 2, 1995, pp. 319–328.
5. Takemoto, Masatsuga, et al.: A Design and Characteristics of Switched Reluctance Type Bearingless Motors. NASA/CP—1998-207654, 1998, pp. 49–63.
6. Takemoto, M., et al.: Improved Analysis of a Bearingless Switched Reluctance Motor. IEEE Trans. Ind. Appl., vol. 37, issue 1, 2001, pp. 26–34.
7. Preston, Mark A., et al.: Integrated Magnetic Bearing/Switched Reluctance Machine. U.S. Patent 5,424,595, June 13, 1995.
8. Morrison, Carlos R.: Bearingless Switched Reluctance Motor. U.S. Patent 6,727,618 B1, Apr. 27, 2004.
9. Marshall, J.T.; Kasarda, M.E.F.; and Imlach, J.: A Multipoint Measurement Technique for the Enhancement of Force Measurement With Active Magnetic Bearings. J. Eng. Gas Turbines Power, vol. 125, no. 1, 2003, pp. 90–94.
10. Knospe, Carl R.; and Maslen, Eric H.: Introduction to Active Magnetic Bearings. A short course presented at NASA Lewis Research Center, Cleveland, OH, Feb. 1999.



Glenn Research Center
National Aeronautics and Space Administration
Cleveland, Ohio, March 24, 2008

# Appendix—Symbols

| | |
|---|---|
| $A$ | General common cross-sectional area between a stator pole and rotor surface ($m^2$) |
| $A^c$ | Common cross-sectional area between a stator pole and circular lamination stack ($m^2$) |
| $A_a$ | Average of $A_b^s$ and $A_c^s$ ($m^2$) |
| $A_b^s$ | Face area of stator pole 1 defined by length of scalloped segment, $2\times10^{-4}$ $m^2$ |
| $A_c^s$ | Surface area inside scallop cavity, $r\theta L^s$, $4.35\times10^{-4}$ $m^2$ |
| $A_k^c$ | Common cross-sectional area between stator pole $k$ and circular lamination stack ($m^2$) |
| $A_k^s$ | Common cross-sectional area between stator pole $k$ and scalloped lamination stack ($m^2$) |
| $A^s$ | Common cross-sectional area between aligned rotor and stator pole ($m^2$) |
| $B$ | General flux density (T) |
| $B_k^c$ | Flux density between stator pole $k$ and circular rotor lamination stack (T) |
| $B_k^s$ | Flux density between stator pole $k$ and scalloped rotor lamination stack (T) |
| $E$ | General energy density between a stator pole and rotor surface ($J/m^2$) |
| $E_k^c$ | Energy density between stator pole $k$ and circular rotor laminations ($J/m^2$) |
| $E_k^s$ | Energy density between stator pole $k$ and scalloped rotor laminations ($J/m^2$) |
| $F_k^c$ | Magnetic force between circular lamination stack and stator pole $k$ (N) |
| $F_k^s$ | Magnetic force between scalloped lamination stack and stator pole $k$ (N) |
| $F$ | Magnetic force (N) |
| $F_{net}^c$ | Net downward magnetic force on circular rotor lamination stack (N) |
| $F_{net}^s$ | Net downward magnetic force on scalloped rotor lamination stack (N) |
| $F_{T(lower)}^c$ | Magnetic force on circular rotor lamination due to stator poles 1, 2, and 8 (N) |
| $F_{T(lower)}^s$ | Magnetic force on scalloped rotor lamination due to stator poles 1, 2, and 8 (N) |
| $F_{T(net\_lev)}$ | Total net magnetic levitating force on the rotor (N) |
| $F_{T(net\_lev)}^c$ | Total net magnetic levitation force on the circular rotor lamination due to stator poles 1, 2, 4, 5, 6, and 8 (N) |
| $F_{T(net\_lev)}^s$ | Total net magnetic levitation force on the scalloped rotor lamination due to stator poles 1, 2, 4, 5, 6, and 8 (N) |
| $F_{t(net)}$ | Total net downward magnetic radial force on rotor (N) |
| $F_{u\_net}^s$ | Net downward magnetic radial force on the unaligned scallop segment (N) |
| $F_{t(u\_net)}$ | Total net downward magnetic radial force on unaligned rotor (N) |
| $F_{T(upper)}^c$ | Magnetic force on circular rotor lamination due to stator poles 5, 4, and 6 (N) |
| $F_{T(upper)}^s$ | Magnetic force on scalloped rotor lamination due to stator poles 5, 4, and 6 (N) |
| $g$ | General gap length between stator pole and rotor (m) |
| $g_a$ | Average stator-rotor gap length at stator pole 1 or 5 (m) |
| $g_b$ | Gap length between a corner edge of the salient stator pole 1 and either of its adjacent rotor salient pole corner edges (m) |
| $g_c$ | Gap length between the midpoint of pole face 1 or 5 and the base of its adjacent scallop cavity (m) |
| $g_k$ | Gap length at stator pole $k$ (m) |
| $g_0$ | Nominal gap length, $5\times10^{-4}$ m |
| $i$ | Current (A) |
| $i_k$ | Current in coil $k$ (A) |
| $L^c$ | Circular rotor lamination stack length, $5.88\times10^{-3}$ m |
| $L^s$ | Scalloped rotor lamination stack length, $1.94\times10^{-2}$ m |
| $l_{tw}$ | Tooth width, $1.03\times10^{-2}$ m |
| $n$ | Number of turns in coil, 215 |
| $P_k$ | Permeance at stator pole $k$ (H) |
| $P_k^c$ | Permeance between stator pole $k$ and the circular rotor lamination stack (H) |
| $P_k^s$ | Permeance between stator pole $k$ and the scalloped rotor lamination stack (H) |

| | |
|---|---|
| $P_T$ | Sum of permeances (H) |
| $P_T^c$ | Sum of permeances at the circular laminations (H) |
| $P_T^s$ | Sum of permeances at the scalloped laminations (H) |
| $R_k^c$ | Reluctance between stator pole *k* and circular lamination stack (1/H) |
| $R_k^s$ | Reluctance between stator pole *k* and scalloped lamination stack (1/H) |
| $R_T^c$ | Total reluctance at circular rotor lamination stack (1/H) |
| $R_T^s$ | Total reluctance at aligned rotor scalloped lamination stack (1/H) |
| $R_{T1}^s$ | Total reluctance at scallop cavity through pole 1 (fig. 10) (1/H) |
| $R_0^s$ | Nominal reluctance at the scalloped segment (1/H) |
| $R_{5\_ratio}^s$ | Reluctance ratio at pole 5 |
| $R_{\|\|}^c$ | Parallel reluctance at circular rotor lamination stack (1/H) |
| $R_{\|\|}^s$ | Parallel reluctance at scalloped lamination stack (1/H) |
| $r$ | Outer radius of rotor laminations (m) |
| $T$ | Torque |
| $V$ | Flux volume between stator pole and rotor ($m^3$) |
| $w$ | Magnetic energy (J) |
| $x$ | Rotor vertical displacement from nominal position (m) |
| $\theta$ | Rotor angle, degrees |
| $\phi_k^c$ | Magnetic flux between stator pole *k* and circular laminations (Wb) |
| $\phi_k^s$ | Magnetic flux between stator pole *k* and scalloped laminations (Wb) |
| $\phi_k$ | Magnetic flux at stator pole *k* (Wb) |
| $\mu_0$ | Permeability of free space, $4\pi\times10^{-7}$ H/m |

| REPORT DOCUMENTATION PAGE | | Form Approved<br>OMB No. 0704-0188 |
|---|---|---|



| 1. REPORT DATE *(DD-MM-YYYY)* | 2. REPORT TYPE | 3. DATES COVERED *(From - To)* |
|---|---|---|
| 01-03-2008 | Technical Paper | |

**4. TITLE AND SUBTITLE**
Electromagnetic Forces in a Hybrid Magnetic-Bearing Switched-Reluctance Motor

**5a. CONTRACT NUMBER**

**5b. GRANT NUMBER**

**5c. PROGRAM ELEMENT NUMBER**

**6. AUTHOR(S)**
Morrison, Carlos, R.; Siebert, Mark, W.; Ho, Eric, J.

**5d. PROJECT NUMBER**

**5e. TASK NUMBER**

**5f. WORK UNIT NUMBER**
WBS 561581.02.08.03.15.02

**7. PERFORMING ORGANIZATION NAME(S) AND ADDRESS(ES)**
National Aeronautics and Space Administration
John H. Glenn Research Center at Lewis Field
Cleveland, Ohio 44135-3191

**8. PERFORMING ORGANIZATION REPORT NUMBER**
E-15821-1

**9. SPONSORING/MONITORING AGENCY NAME(S) AND ADDRESS(ES)**
National Aeronautics and Space Administration
Washington, DC 20546-0001

**10. SPONSORING/MONITORS ACRONYM(S)**
NASA

**11. SPONSORING/MONITORING REPORT NUMBER**
NASA/TP-2008-214818

**12. DISTRIBUTION/AVAILABILITY STATEMENT**
Unclassified-Unlimited
Subject Categories: 33 and 70
Available electronically at http://gltrs.grc.nasa.gov
This publication is available from the NASA Center for AeroSpace Information, 301-621-0390

**13. SUPPLEMENTARY NOTES**
Submitted to Journal of IEEE Transactions on Magnetics

**14. ABSTRACT**
Analysis and experimental measurement of the electromagnetic force loads on the hybrid rotor in a novel hybrid magnetic-bearing switched-reluctance motor (MBSRM) have been performed. A MBSRM has the combined characteristics of a switched-reluctance motor and a magnetic bearing. The MBSRM discussed in this report has an eight-pole stator and a six-pole hybrid rotor, which is composed of circular and scalloped lamination segments. The hybrid rotor is levitated using only one set of four stator poles, while a second set of four stator poles imparts torque to the scalloped portion of the rotor, which is driven in a traditional switched reluctance manner by a processor. Static torque and radial force analysis were done for rotor poles that were oriented to achieve maximum and minimum radial force loads on the rotor. The objective is to assess whether simple one-dimensional magnetic circuit analysis is sufficient for preliminary evaluation of this machine, which may exhibit strong three-dimensional electromagnetic field behavior. Two magnetic circuit geometries, approximating the complex topology of the magnetic fields in and around the hybrid rotor, were employed in formulating the electromagnetic radial force equations. Reasonable agreement between the experimental and the theoretical radial force loads predictions was obtained with typical magnetic bearing derating factors applied to the predictions.

**15. SUBJECT TERMS**
Bearingless motor; Electromagnetic device; Hybrid motor; Magnetic field calculation; Switched-reluctance motor; Motor; Magnetic bearing; Electromagnetic equations

| 16. SECURITY CLASSIFICATION OF: | | | 17. LIMITATION OF ABSTRACT | 18. NUMBER OF PAGES | 19a. NAME OF RESPONSIBLE PERSON |
|---|---|---|---|---|---|
| a. REPORT | b. ABSTRACT | c. THIS PAGE | | | STI Help Desk (email:help@sti.nasa.gov) |
| U | U | U | UU | 21 | 19b. TELEPHONE NUMBER *(include area code)*<br>301-621-0390 |